Applied Research

RESEARCH ARTICLE OPEN ACCESS

TER-Ox: Simultaneous Monitoring of Epithelial Barrier Function (TER) and Mitochondrial Respiration (Ox)

Tobias Naber[1,2] | Katharina Winter[2] | Joachim Wegener[1,2]

[1]Division Cell-Based Sensor Technology, Fraunhofer Institute for Electronic Microsystems and Solid State Technologies EMFT, Regensburg, Bavaria, Germany | [2]Institute for Analytical Chemistry, Chemo- & Biosensors, University of Regensburg, Regensburg, Bavaria, Germany

Correspondence: Joachim Wegener (Joachim.Wegener@ur.de)

Received: 24 July 2024 | **Revised:** 13 November 2024 | **Accepted:** 20 December 2024

Keywords: epithelial barrier function | impedance spectroscopy | microphysiometry | oxygen consumption rate | ratiometric optical imaging | respiratory activity | transepithelial electrical resistance

ABSTRACT

Epithelial barrier function and cellular respiration are key cellular phenotypes in health and disease and as such involved in the progression of many pathological disorders. Accordingly, the molecular drivers are targeted extensively in drug development using appropriate disease models in vitro. So far, quantification of barrier function and metabolic respiration had to be conducted in individual phenotypic assays, making it impossible to track changes simultaneously in a single cell layer over longer periods. We have developed an assay platform that allows for simultaneous monitoring of both, the epithelial barrier function and metabolic activity of cell layers cultured on permeable substrates label-free and non-invasively. Therefore, we designed a stainless-steel measurement chamber capable of combining impedance spectroscopy and ratiometric fluorescence-based oxygen mapping. In this platform, the barrier function is quantified as the *transepithelial electrical resistance* (TER) while the respiratory activity is expressed as the *apparent oxygen consumption rate* (AOCR) yielding the name TER-Ox for the combined setup. We validated the TER-Ox system by studying the epithelial cell lines MDCK-I, MDCK-II, and A549, covering a wide range of barrier tightness. Results of the combined TER-Ox setup were compared to established but individual readouts of barrier function (cellZscope®) and oxygen consumption (VisiSens TD®). Also, we show that differences in both parameters are readily monitored while treating cell layers with modulators affecting the electron transport chain (Antimycin A and malonoben) or barrier integrity (Cytochalasin D).

1 | Introduction

Barrier function and cellular respiration are two characteristic indicators for epithelial polarization and metabolic activity, respectively. Alterations of both, individually and in combination, are often phenotypic hallmarks of different pathologies that are readily studied in appropriate disease models in vitro. Prominent examples are *epithelial-to-mesenchymal-transition* (EMT), which is often the starting point of cancer metastasis, or many types of fibrosis [1, 2]. In the case of EMT for example, the epithelial de-differentiation of cells is generally associated with a loss of barrier function and strong metabolic changes [3, 4]. Hence, experimental monitoring of changes occurring in respiratory activity and barrier function may enable identification of the molecular drivers and assist significantly during the corresponding drug development processes.

Quantification of both parameters, *transepithelial electrical resistance* (TER) and *apparent oxygen consumption rate* (AOCR), is usually performed with separate devices since no experimental platforms exist allowing for easy and reliable simultaneous analysis. Currently, the gold standard for determining cellular respiration non-invasively and label-free is the Seahorse™ device. It is based on a ratiometric assessment of

fluorescence emission using a combination of oxygen-sensitive and -insensitive luminophores. The device integrates over the whole cell layer without any spatial resolution, ignoring local changes in oxygen consumption characteristics [5]. Other devices rely on the electrochemical detection of dissolved oxygen by applying miniaturized Clark-type electrodes for amperometric quantification [6, 7]. The downside of electrochemical techniques is that oxygen is chemically converted during analysis and thereby consumed. Generally, these assays are used to study cell populations grown on impermeable, solid substrates. However, many epithelial cell types only fully polarize when grown on permeable, porous culture substrates (referred to as filters), as this enables the cells to develop cell polarity [8] and to actively establish chemical gradients between the apical and basolateral fluid compartment [9]. Additionally, assays addressing permeability and transport of solutes across epithelial barriers inevitably rely on cells cultured on permeable substrates [10–12].

Quantifying barrier function of cells grown on permeable substrates is dominated by electrical resistance or impedance readouts, both providing the TER as a measure for the cell layer's permeability for inorganic ions like Na^+, K^+ or Cl^-. TER readings provide instantaneous, time-resolved information on barrier function, they allow for repeated measurements and they are independent of any labels. The common feature of these platforms is the use of electrodes which are placed in the fluid compartments on opposite sides of the cell layer [13]. The most frequently used system, the chopstick electrodes, is based on the application of single-frequency square wave currents (12.5 Hz) between apical and basolateral electrodes. The associated short-term electrochemical polarization of the cell layer apparently does not harm the cells. However, chopstick electrodes are known to overestimate TER values since their point-like structure produces inhomogeneous electric fields across the cell layer. This phenomenon gets increasingly important when filter substrates with larger surface areas are used [14]. Additionally, care must be taken to not disturb or destroy the cell layer when repeatedly placing chopstick electrodes on either side of the cell layer what is typically done outside of the incubator at room temperature. Many of these issues are eliminated by systems that use planar electrodes for current injection [15]. Impedance analysis applied in multi-well formats to filter grown cell layers inside a regular cell culture incubator, as enabled by the cellZscope® or TEER Z® device, provides an alternative to the chopstick approach described above. In general, these platforms benefit particularly from invariant electrode positions and hence better reproducibility, a stable undisturbed environment for the cells inside the incubator, the non-invasiveness of small amplitude AC currents, the option for time-resolved online monitoring and the scalability from 6well to 96well formats [13, 16]. Moreover, impedance measurements along a wide range of AC frequencies, as provided by the cellZscope® platform, also return the cell layer capacitance which serves as an indicator for changes in plasma membrane topography like microvilli and membrane invaginations as the membrane capacitance directly scales with the plasma membrane surface area. The latter are also quantitative indicators for epithelial polarization [9].

Examples of label-free and noninvasive monitoring of respiration and epithelial barrier function of the same cell layer cultured on permeable substrates are rare and are mainly based on microfluidic setups in organ- or lab-on-a-chip approaches [17, 18]. However, these systems often suffer from low throughput as well as a high technical complexity of the set-up. The assay platform we present in this study is capable of determining epithelial barrier function and mitochondrial respiration of the same cell population simultaneously, noninvasively and with a time resolution of several minutes. To apply this platform, the cells of interest are cultured in commercially available cell culture inserts with a highly porous growth surface as they are typically used to study epithelial or endothelial physiology. No special treatments or culture conditions are required. The oxygen readout is based on an imaging technique mapping the local oxygen consumption within a given cell layer. The barrier function is determined by impedance spectroscopy with inherent equivalent circuit modeling so that TER and membrane capacitance are returned by the measurement.

2 | Methods

2.1 | Cell Lines and Culture Conditions

All cell culture work was carried out in a laminar airflow cabinet (Thermo Fischer Scientific Inc, USA) to ensure sterile conditions. Cell lines were routinely cultured in T25 flasks (Greiner BioOne, Germany) in a standard cell culture incubator at 95% relative humidity, 5% CO_2, and 37°C. Cell lines were subcultivated once a week at approximately 80%–90% confluency. Medium was refreshed every 3 days. Substances and solutions were purchased from Merck kG if not stated otherwise. All solutions were pre-warmed to 37°C before use. Subcultivation was performed using a standard protocol including EDTA treatment followed by trypsination. MDCK-I and MDCK-II cells were cultured in DMEM containing 4.5 g/L glucose supplemented with 10% FCS, 4 mM glutamine, 100 µg/mL streptomycin, and 100 units/mL penicillin. A549 cells were cultured in Ham's F12 supplemented with 5% FCS, 2 mM glutamine, 100 µg/mL streptomycin, and 100 units/mL penicillin. MDCK-I and MDCK-II cells were provided by the research group of Prof. Galla (Institute for Biochemistry, University of Muenster, Germany). A549 cells were obtained from the research group of Prof. Heilmann (Institute for Pharmacy, University of Regensburg). For experiments, cell suspensions were diluted in the respective culture medium and seeded on Transwell® filter substrates (growth area: 0.33 cm^2, pore diameter: 0.4 µm, pore density 10^8 pores/cm^2, polycarbonate, Costar Corning, LMS Consult, Germany) at a density of 5×10^5 cells/cm^2. Apical and basolateral medium was exchanged after 24 h. After 48 h, the medium was aspirated, and cells were washed once with Leibovitz L-15 medium (+100 units/mL penicillin and 100 µg/mL streptomycin). For analysis, cells were incubated in L-15 (+100 units/mL penicillin and 100 µg/mL streptomycin) and transferred to the TER-Ox measurement chamber. Antimycin A, malonoben, and cytochalasin D were stored as stock solutions in DMSO at −20°C and were freshly diluted to working concentrations before each measurement.

2.2 | TER-Ox Assay

To measure both, the local oxygen consumption (Ox) and integral barrier function (TER) of epithelial cell layers, we combined two fundamental measurement principles in one setup and coined the term *TER-Ox* for this mode of combined analysis. The barrier-forming phenotype is characterized by impedance spectroscopy resulting in the TER and the cell layer capacitance (C_{Cl}). Before the measurement, the cell-covered inserts are placed between an apical dipping electrode and a basolateral pot electrode. This two-electrode-configuration is justified as there is no electrochemical reaction and thus, no faradaic current across the electrode/electrolyte interface. Both electrodes were made from stainless steel and behave close to ideally polarizable electrodes. Impedance was recorded by applying an alternating voltage of 50 mV amplitude at distinct frequencies within a range from 1 Hz to 100 kHz, while the corresponding current was measured. Impedance spectra of the cells have been recorded repeatedly resulting in a time-resolved profile of changes in barrier function or membrane topography. The oxygen concentration is mapped by using the VisiSens TD® system (PreSens Precision Sensing, Regensburg, Germany) for ratiometric optical imaging yielding time-resolved oxygen maps. To enable optical imaging of oxygen consumption of the same cell layer, an optical window was introduced in the basolateral electrode of every well for fluorescence excitation and detection (Figure 1A).

An oxygen-sensitive foil is placed inside these windows. The foils consist of an oxygen-permeable polymer doped with a sensing fluorophore (red), whose luminescence is readily quenched by dissolved oxygen, and a reference fluorophore (green) that is insensitive to oxygen. The ratio of both indicates specifically the local level of oxygen in every pixel of the recorded image. For quantification, the system has been subjected to a two-point calibration using a medium that was fully saturated with air (100% dissolved O_2) and a medium without oxygen (0% dissolved O_2). The 0% dissolved O_2 calibration was conducted using a measurement buffer containing 10 g/L sodium sulfite for complete reduction of the available oxygen while 100% dissolved O_2 is represented by an oxygen saturated L-15 solution. The oxygen imaging was controlled via the VisiScientifical Software (PreSens Precision Sensing, Germany).

For the measurement, the TER-Ox chamber was directly placed on top of the VisiSens TD® camera system inside a non-humidified incubator at 37°C (Figure 1B). The electrodes of the chamber were connected to a relay to individually address the apical electrodes of different wells. Impedance data was recorded using a Solartron impedance analyzer SI 1260 (Solartron, UK). Measurement of the electrochemical impedance and data storage was controlled by self-written software based on LabView. Analysis of the raw data for the two measurement modes is described individually below.

2.3 | Design of the TER-Ox Chamber

The final TER-Ox chamber (Figure 2E) enables the combination of broad-band impedance analysis and optical oxygen mapping underneath epithelial cell layers. The bottom or basolateral chamber consists of four major layers (Figure 2A), which are assembled and fixed by five screws from the bottom side. The first layer is a stainless-steel plate (l = 5.6 cm, w = 8.7 cm, h = 1.9 mm) serving as support for the entire set-up. This supporting plate has four circular holes (d = 1.6 cm) serving as optical windows to perform optical oxygen mapping. The second layer is a Lexan® plate (l = 5.6 cm, w = 8.7 cm, h = 0.5 mm, type 8010 MC colorless 112 polish, alt-intech) carrying four circular spots (d = 7 mm) of the oxygen sensor foil (SF-RPSu4, PreSens Precision Sensing GmbH, Germany). The sensor foils are glued upon the Lexan® plate in positions exactly matching the optical windows in the support plate using biocompatible silicon glue (RS Components Ltd, UK). On top of the Lexan® plate, we apply a second stainless-steel plate with a thickness of approximately 100 µm matching the thickness of the oxygen sensor foil. This plate also has a set of four circular holes at the dimensions and position of the oxygen sensor spots.

This ensures the contact of the sensor foil to the cell culture medium. To complete the basolateral setup, we fix a stainless-steel block (l = 5 cm, w = 5 cm, h = 1.645 mm) with four cylindrical openings to the bottom plate. The openings form basolateral fluid compartments and serve as basolateral pot electrodes together with the stainless-steel bottom plate (Figure 2B). The cell-covered, porous cell culture inserts are directly hanging inside the cylindrical openings of the basolateral

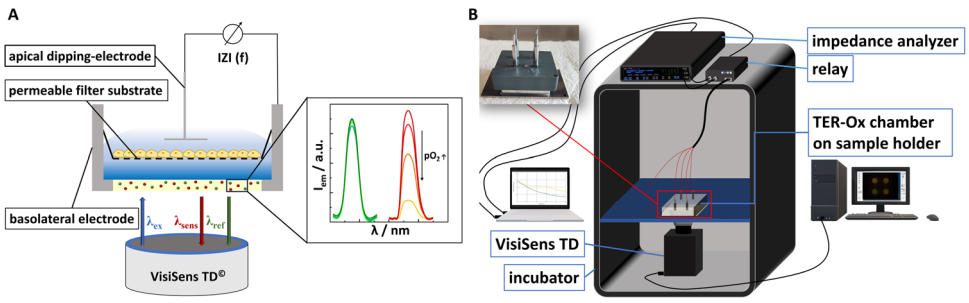

FIGURE 1 | Principle and setup of the TER-Ox assay. (A) Schematic side view of a well of the TER-Ox plate with the apical and basal electrodes as well as the oxygen-sensitive foil underneath the cell-covered Transwell™ filter. The graphical insert highlights luminescent intensities of reference and sensing fluorophore for increasing oxygen concentrations. (B) Schematic illustration of the completed TER-Ox setup, consisting of the TER-Ox chamber, the VisiSens TD camera system for oxygen mapping, a relay, an impedance analyzer as well as ordinary computers for measurement controls. The setup currently relies on two individual PCs as the instrument controls for both measurement modes require individual operating systems.

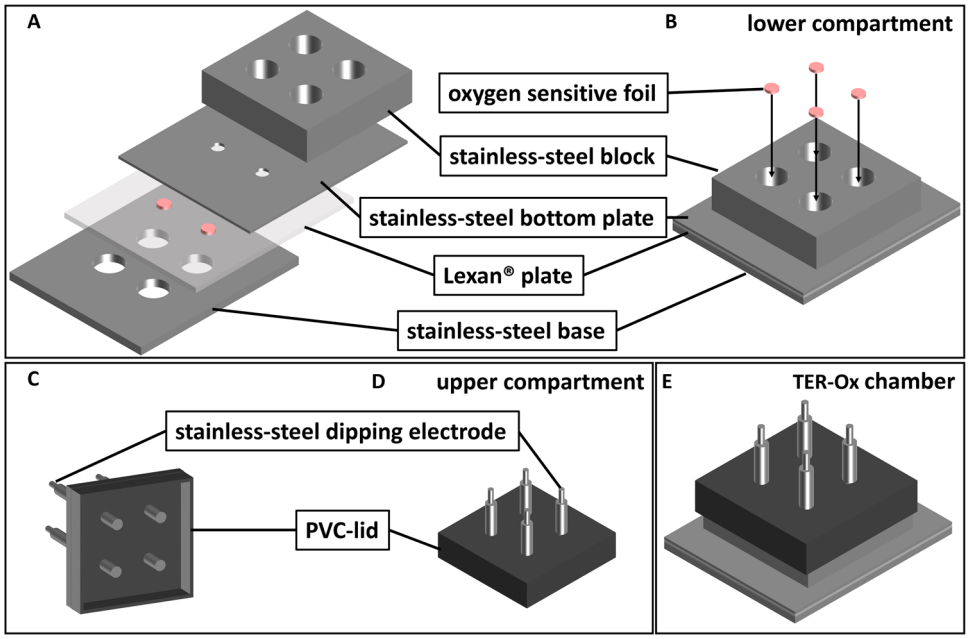

FIGURE 2 | Design and assembly of the TER-Ox measurement chamber (A) Different layers of the basolateral chamber setup: Stainless-steel base for support with four circular openings used as optical windows; Lexan® plate with spots of a commercial oxygen sensor foil; stainless-steel plate and stainless-steel block serving as basolateral pot electrode. (B) Fully assembled basolateral part of the chamber. (C) Bottom view of the apical part of the chamber, consists of a PVC lid and four individually addressable stainless-steel dipping electrodes. (D) Top view of the apical part of the chamber. (E) Fully assembled TER-Ox chamber.

chamber. To prevent leakage out of the chamber or between the four layers, the contact areas between the stainless-steel plate and the Lexan plate, as well as the stainless-steel plate and the stainless-steel block, are sealed using a layer of silicon fat (KORASINOL-Paste, Kurt Obermeier GmbH & co. KG) and a silicon rubber ($l = 5$ cm, $w = 5$ cm, $h = 1$ mm, Product-Nr.: 240,000,100, Technischer Handel Straub), respectively.

The apical part completes the setup. It holds the four individual dipping electrodes necessary for impedance measurements across the cell layer while also serving as a lid. Therefore, we designed a PVC lid with four drill holes. The drill holes are used to fix the stainless-steel dipping electrodes ($d = 4.5$ mm), which are glued into the drill holes using silicon glue (Figure 2C,D).

2.4 | Data Evaluation

Impedance spectra were analyzed by fitting the parameters of an equivalent circuit to the raw data (Figure 3). In this equivalent circuit, the dielectric properties of the electrochemical system (electrodes/cell layer/porous insert/medium) are represented by a network of individual impedance elements [19]. The resistance of the culture medium is represented by an *ohmic resistor* R_{Med}; the impedance of the electrodes is accounted for by a *constant phase element* (CPE). The dielectric properties of the porous cell culture insert and the cell layer are individually represented by a parallel combination of a capacitor and a resistor. In case of the porous support, the impedance elements are R_{Ins} and C_{Ins} (Ins = insert). The layer of barrier-forming cells is accounted for by the resistor TER and the capacitor C_{Cl} (Cl = cell layer). The latter two parameters are the experimental descriptors of the cell layer under study. The parameters of this AC circuit's transfer function are fitted to the experimental spectra using a numerical optimization algorithm coded in Matlab®. The whole procedure results in values for the TER and the cell layer capacitance C_{Cl}. These two parameters are quantified for each spectrum leading to time-resolved datasets of both quantities.

To evaluate the micrographs taken by the VisiSens TD system (Figure 4), the oxygen sensor spot is first calibrated using a simple two-point calibration as described above. The ratio of red and green luminescence is calculated for each pixel of the recorded micrographs. Based on the calibration, the individual luminescence ratios are then converted to a corresponding local oxygen partial pressure (pO_2) at the surface of the sensor spot. This procedure yields time-resolved maps of lateral oxygen distribution. By defining *regions of interest* (ROI) in the micrographs and subsequently analyzing the stack of maps recorded at this position along the experiment, the local oxygen partial pressure in this pixel above the sensor foil is accessible as a function of time. Analysis is performed using the VisiSens Scientifical Software (PreSens Precision Sensing GmbH, Germany). The AOCR is extracted from these time courses by calculating the slope of the curve during the phase of linear decrease with time.

2.5 | cellZscope® Measurements

For benchmarking the TER-Ox device, comparative measurements of the TER were conducted using the cellZscope® 3 device (nanoAnalytics; Germany). After washing, cells were transferred to the cellZscope® device and monitored for 12 h every 5 min in L-15 medium using default settings. TER and C_{Cl}

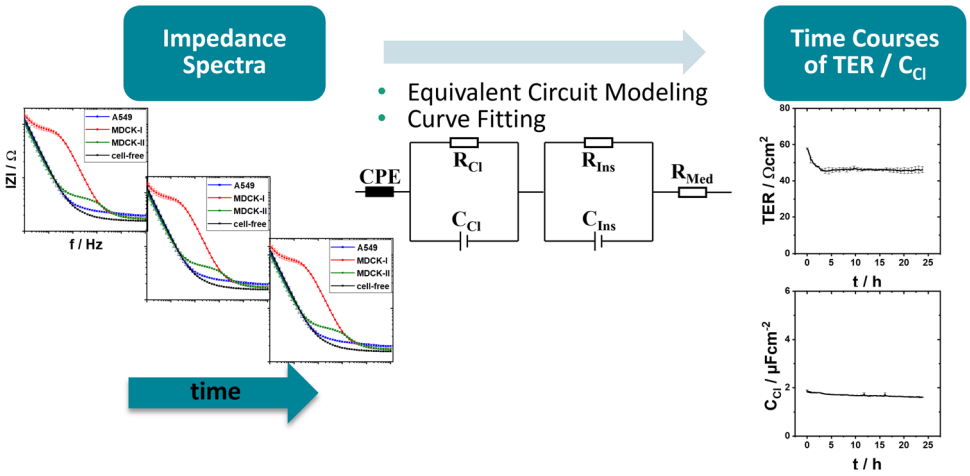

FIGURE 3 | Data evaluation of impedance measurements. The spectra are analyzed by means of equivalent circuit modeling, yielding values for the resistance (TER) and the capacitance of the cell layer (C_{Cl}). Fitting is performed using a numerical optimization algorithm coded in Matlab®.

values were extracted after 10 h for comparison to the outcome of the TER-Ox assay.

2.6 | VisiSensTD® Measurements

Similar benchmarking experiments regarding the quantification of AOCR were conducted using the standard VisiSens TD® system (PreSens Precision Sensing GmbH, Germany). Commercial oxygen-sensor spots (SF-RPSu4, PreSens Precision Sensing GmbH, Germany) were glued into the wells of standard 24-well cell culture plates (Greiner BioOne, Germany). After placing cell-covered inserts into the wells of the 24-well plate, local oxygen partial pressures were monitored for 3 h by repeated acquisition (every 10 min) of ratiometric images as described above. AOCRs were determined as described above and compared to TER-Ox measurements.

3 | Results & Discussion

3.1 | Simultaneous Monitoring of TER and AOCR

To demonstrate the functionality of the TER-Ox setup, three popular epithelial cell lines with distinctly different barrier functions have been studied: (i) A549 derived from human adenocarcinoma of the lung, (ii) MDCK-II derived from canine kidney, and (iii) MDCK-I also derived from canine kidney but from a different part of the tubulus compared to MDCK-II.

A549 cells form very leaky barriers and are widely used in assays addressing mitochondrial respiration. We typically found TER values of around 6 $\Omega\,cm^2$ (Figure 5A) which is in line with the literature, reporting TER values below 30 $\Omega\,cm^2$ [20, 21]. The *cell layer capacitance* C_{Cl} was quantified to 1.4 $\mu F/cm^2$ indicating the expression of membrane protrusions like microvilli on the apical surface or invaginations on the basolateral surface. This interpretation is based on the fact that a cell with entirely flat membrane topography shows a *membrane capacitance* of 1 $\mu F/cm^2$. This value is independent of cell type [16]. The current has to pass two membranes on the transcellular path across the cell layer—namely the apical and the basal membrane. Since the two membrane capacitances C_{Ap} and C_{Bl} are in series, the total capacitance of a *cell layer* with entirely flat membranes C_{Cl} is 0.5 $\mu F/cm^2$ ($1/C_{Cl} = 1/C_{Ap} + 1/C_{Bl}$). These C_{Cl} values have been often found for endothelial cells [16, 22]. Or vice versa: a cell layer capacitance of 1.4 $\mu F/cm^2$ as determined for A549 cells translates into an *average* membrane capacitance of $C_{Ap} = C_{Bl} = 2.8\,\mu F/cm^2$ for the apical and the basal plasma membrane, respectively, if we assume that both membrane domains contribute equally. Any other combination of C_{Ap} and C_{Bl}, yielding the observed C_{Cl} according to the equation given above, is also possible. Since the capacitance scales with the area, the apical and basal sides of A549 cells have approximately three times the membrane surface area compared to their projections onto the growth surface (= footprint) if $C_{Ap} = C_{Bl} = 2.8\,\mu F/cm^2$ holds true. This enlargement of the plasma membrane surface is a phenotypic hallmark of transporting epithelia [22]. Since the membrane capacitance is not affected significantly by, for instance, protein content or other parameters that are standardized in animal cell culture, the capacitance can be interpreted directly as a measure of plasma membrane surface area [23].

MDCK-II cells are often used as a model for a moderately tight epithelial barrier with active transcellular solute transport [24]. Formation of a moderately tight barrier was confirmed using the TER-Ox setup, resulting in TER values around 50 $\Omega\,cm^2$ (Figure 5B) which is slightly lower than published values [19, 25] but still in the same order of magnitude below 100 $\Omega\,cm^2$. The average cell layer capacitance C_{Cl} amounts 1.7 $\mu F/cm^2$, which is even higher than observed for A549 cells but slightly lower than reported for this cell type in the literature [19, 25]. It is our experience that MDCK-II cells are easy to grow and maintain in culture for weeks or even months without re-starting the culture from a fresh cryopreserved stock culture. TER and C_{Cl} values may drift or scatter along an extended time in culture for reasons that we can only speculate about. Thus, we have performed an independent impedance analysis of all cell lines under study to ensure correct readings with the TER-Ox device. The results are summarized below.

The MDCK-I cell line is commonly used to emulate tight epithelial barriers [26] with high TER values and low permeation

rates for molecular markers (P_E). Accordingly, TER-Ox studies returned by far the highest TER values for MDCK-I cell layers. After a strong decrease of the TER in the first 2 h of a typical time course experiment, values equilibrate around 1400 Ω cm^2 (Figure 5C). To the best of our knowledge, this initial strong decrease in TER from more than 5000 to 1400 Ω cm^2 shortly after the cells have been transferred into the TER-Ox setup, is a response of the cells to (i) liquid handling, (ii) the inevitable change of incubation buffers from serum-containing cell culture medium to L-15 minimal medium together with (iii) the associated temperature disturbances. MDCK-I cells responded dramatically to a change in the incubation buffer and the L-15 medium had to be supplemented with 4.5 g/L glucose for cell layer stabilization. Without the addition of glucose, the TER values dropped continuously below 1000 Ω cm^2 (Supporting Information: Figure S1B). However, the change of incubation buffer was necessary since measurements with the TER-Ox setup in our lab currently require a CO_2 free atmosphere and buffer systems adapted thereto. Similar results were obtained when an independent impedance analysis device (cellZscope®) was used. These studies returned similar time courses for MDCK-I cells (Supporting Information: Figure S1A). The cell layer capacitance C_{Cl} of MDCK-I cell layers was quantified to 1.6 μF/cm^2 on average. It is slightly lower than C_{Cl} of MDCK-II cells as it has been reported before [25].

The time courses of the oxygen partial pressure pO_2 show a similar curve characteristic for all three cell lines starting at values of cell culture fluid fully equilibrated with ambient air (app. 120 torr). Differences for the individual cell lines arise in the slope of the time course within the first 4 h as well as the equilibrium values (Figure 5A–C). As indicated in Figure 4, the AOCR is individually determined from the slope of the linear part of the curve after the temperature-induced transient maximum. AOCR for A549 cells amounts to (25.1 ± 0.6) amol/(s*cell). MDCK-II cells show an average respiration rate of (37 ± 5) amol/(s*cell). Measurements returned a rather similar respiration rate for MDCK-I as for MDCK-II cells, which is (38 ± 8) amol/(s*cell). These AOCRs are all within the range of results reported in literature [27, 28]. These values indicate for all three cell lines that their energy consumption relies to a significant part on aerobic metabolism.

3.2 | Comparison to Established Monitoring Platforms

To validate the results measured with the TER-Ox setup, we compared the values for AOCR, TER, and C_{Cl} to data recorded with established commercial devices: (i) VisiSens TD for respiration and (ii) cellZscope® for barrier function. The AOCRs reported by TER-Ox are in line and not significantly different from the results obtained using VisiSens TD (Figure 6A) supporting our hypothesis that neither AOCR-readings nor the cells are affected by the presence of stainless steel electrodes or other elements of the TER-Ox setup. TER values of A549 cells and MDCK-II cells obtained in TER-Ox experiments were also in good agreement with the corresponding cellZscope® assays. It is important to note that TER values respond very sensitively to slight mechanical disturbances, temperature drifts or any kind of liquid handling. In comparison to the pool of TER values recorded in our laboratory, the observed differences are within the regular data scattering recorded for these two cell lines with different devices. For MDCK-I cells, we observed significant differences between the TER values recorded with TER-Ox or cellZscope®, respectively. As described above, TER is rather sensitive to slight variations in cell culture parameters. This is particularly true for very tight epithelial or endothelial cell layers with high TER values. Similar observations have been made with endothelial cells derived from brain capillaries forming the blood-brain barrier in vivo [29] or other tight barrier-forming cell species. The reader may get a vivid impression of this sensitivity by looking at the time course of TER readings reported in Figure 5C for this cell type. Immediately after introducing the cell-covered filter insert into the TER-Ox setup, TER values for this cell type are close to 5 kΩ cm². During equilibration, the values decrease and stabilize at 1.3 kΩ cm² within less than 2 h. At the same time, the oxygen consumption is not significantly different compared to MDCK-I cells studied independently in the VisiSens TD setup indicating that the cells have not been treated differently compared to other assays. Despite the differences for MDCK-I cells, the general trend of TER values was similar for both methods and readings clearly distinguish between low (A549), moderate (MDCK-II) and tight (MDCK-I) barrier function.

Comparing the cell layer capacitances C_{Cl} as recorded by TER-Ox or cellZscope® we found differences in the A549 cells' values, whereas the results for MDCK-II and MDCK-I cells are in line, showing that an intact layer was formed with the expression of microvilli and/or other convolutions of the plasma membrane (Figure 6C). The differences found for A549 cells are most likely attributed to the extremely leaky barrier that these cells form. The very weak impact of these cell layers on the total impedance of the system leads to difficulties during the fitting procedure. To effectively measure impedance spectra for A549 cells, the area of the filter membrane needs to be decreased in future measurements, allowing a more sensitive TER determination. The reader is referred to Supporting Information: Table S1 for studying the individual readings that contributed to averaging.

3.3 | Monitoring the Influence of Electron Transport Chain and Barrier Function Modulators

In the last set of experiments, we treated MDCK-II cells independently with two specific electron transport chain modulators and a barrier function modulator (Figure 7). *Antimycin A* is a blocker of complex III of the electron transport chain which leads to a minimization of cellular respiration [30]. The TER-Ox results show that MDCK-II cells stopped oxygen consumption when treated with antimycin A (2 μM) as the time course of oxygen partial pressure does not show any decrease (Supporting Information: Figure S2). Thus, AOCR cannot be calculated anymore and is set to 0 amol*(s*cell)$^{-1}$. Antimycin A also showed strong influences on the tightness of the epithelial barrier. Immediately after addition, cells seemed to react to the treatment by a tightening of the cellular barrier leading to a strong increase in TER. Additionally, cells seemed to partially

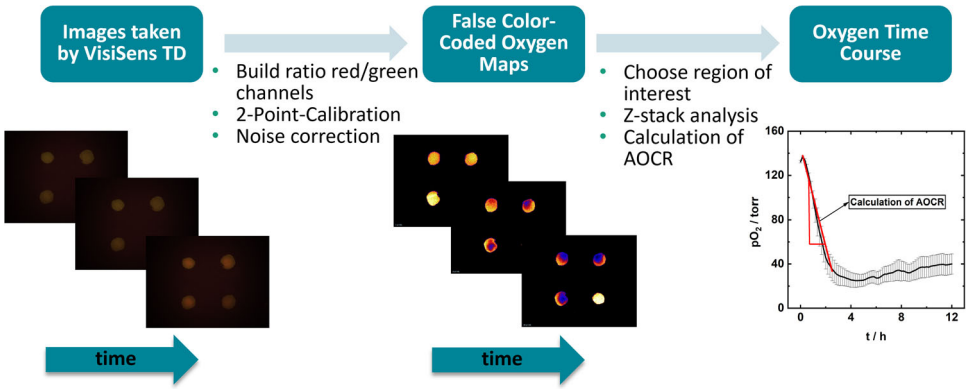

FIGURE 4 | Data evaluation of microscopic oxygen maps using the VisiSens TD system. The images are completely analyzed using the software provided by PreSens Precision Sensing GmbH. After image acquisition, the sensor foil is calibrated using a two-point calibration (0% dissolved O_2, 100% dissolved O_2). Based on this calibration the ratio of red and green luminescence is converted to a local oxygen partial pressure for each pixel resulting in false-color-coded oxygen maps. Analysis of pre-defined ROIs inside the oxygen maps results in time-resolved changes in oxygen partial pressure for this ROI at the surface of the sensor spot beneath the cell layer. The apparent oxygen consumption rate (AOCR) is determined from the slope of the linear part of the time course.

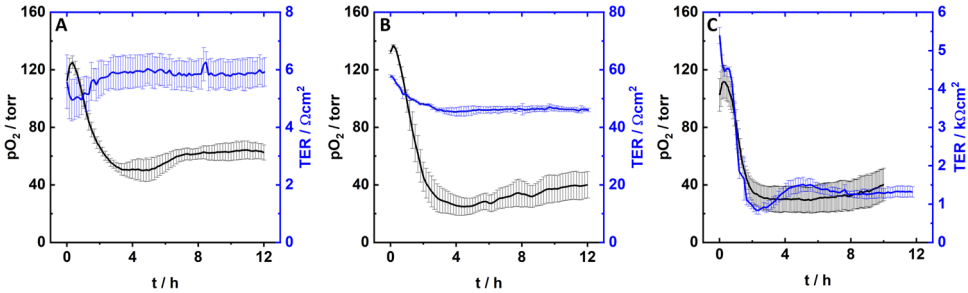

FIGURE 5 | Simultaneous monitoring of epithelial barrier function and respiratory activity of A549, MDCK-II and MDCK-I. Partial oxygen pressure (black) and transepithelial electrical resistance (blue) time courses of (A) A549 cells, (B) MDCK-II cells and (C) MDCK-I cells. TER and pO_2 were monitored simultaneously using the TER-Ox setup in a dry cell culture incubator at 37°C and 0% CO_2 (Mean ± SEM, $n = 3$).

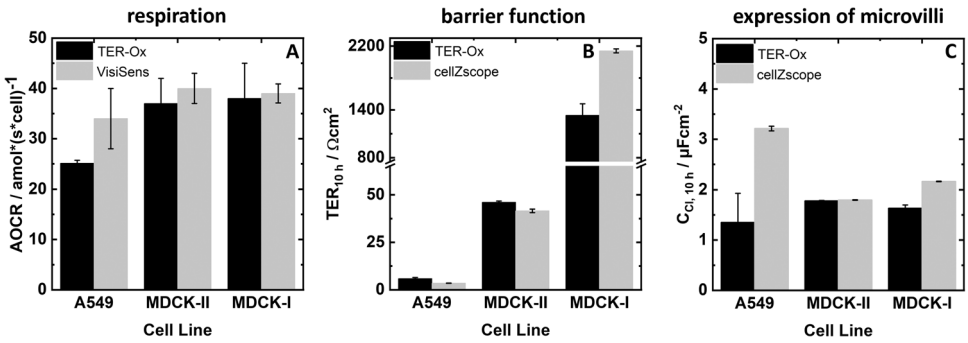

FIGURE 6 | Comparison of results obtained in TER-Ox measurements to the established VisiSens TD (cellular respiration) and cellZscope® (barrier function) assays. (A) Apparent oxygen consumption rates determined by TER-Ox and VisiSens experiments. (B) TER values and (C) capacitance values after 10 h, resulting from TER-Ox and cellZscope® measurements. All results were obtained in a dry cell culture incubator at 37°C and 0% CO_2 in three individual experiments (Mean ± SEM, $n = 3$).

lose their pre-established microvilli indicated by a decrease in cell capacitance C_{Cl} with time. After the initial reaction, antimycin A initiates cell death, leading to a decrease of the TER followed by a strong increase in cell layer capacitance due to cell detachment. When the cell layer gets permeable, readings of the capacitance fail in all devices that rely on impedance analysis. *Malonoben*, an uncoupler of the electron transport chain, is reported to enhance cellular oxygen uptake to a maximum by short-circuiting the proton gradient which is established across the inner mitochondrial membrane by the ETC [31]. Accordingly, using TER-Ox we saw a strong increase in the AOCR, while neither epithelial barrier nor the membrane topography was affected by exposure to malonoben (10 nM). *Cytochalasin D* is a disruptor of actin filament network organization, resulting in a significant reduction of barrier tightness and microvilli dimensions [32]. TER-Ox results show a strong

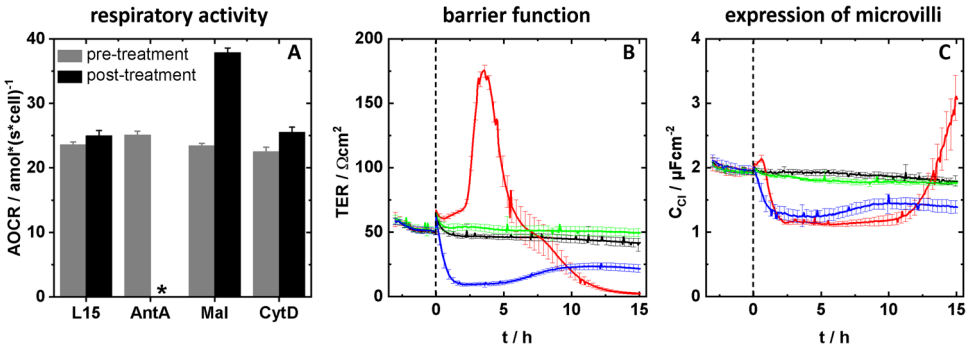

FIGURE 7 | Treatment of confluent MDCK-II cell layers with electron transport chain and barrier function modulators. Cells were treated with an L15 buffer control, antimycin A (2 µM)S, malonoben (10 nM), or cytochalasin D (5 µM), respectively. (A) Influence of antimycin A (Ant A), malonoben (Mal), and cytochalasin D (CytD) on respiratory activity of MDCK-II cells as measured by the apparent oxygen consumption rate (AOCR). (B), (C) Influence of L15 buffer control (back), antimycin A (**red**), malonoben (**green**), and cytochalasin D (**blue**) on barrier integrity and membrane topography of MDCK-II cells as reported by TER and C_{Cl}. The modulating compounds were added at t = 0 h (dashed line). All results were obtained using TER-Ox in three individual experiments in a dry cell culture incubator at 37°C and 0% CO_2 (Mean ± SEM, n = 3).

decrease in TER values as well as the cell layer capacitance. TER decreased due to the loss of cell-cell contacts, whereas capacitance decreased due to a reduction of microvilli on the apical surface. However, the cells do not detach from the surface of the Transwell® inserts and the monolayer stays intact as indicated by the rather time-invariant cell layer capacitance towards the end of the experiment. Moreover, the respiratory activity of MDCK-II cells was not influenced by cytochalasin D (5 µM) addition. The reader is referred to Supporting Information: Figure S2 for studying the individual time courses of pO_2 that contributed to the averaged AOCR values in 7 A.

4 | Conclusions & Outlook

We successfully developed an experimental platform capable of simultaneously monitoring cellular respiration and barrier integrity of cell layers cultured on porous substrates using a combination of ratiometric optical imaging and electrochemical impedance spectroscopy. To the best of our knowledge, TER-Ox is the first device to allow for microphysiometry measurements on cell layers grown on permeable substrates. We were able to show, that the novel TER-Ox platform provided similar results as state-of-the-art methods for individual and independent quantification of oxygen consumption (ratiometric optical imaging) and epithelial barrier function (cellZscope®) as well as trends reported in literature. However, we also realized, that cell layers forming very leaky barriers require particular attention during equivalent circuit modeling. In the future, we are planning to overcome these issues by a reduction of the substrate area leading to a higher sensitivity of the impedance readout. Our results show that TER-Ox is suitable to determine drug-induced changes within a cell layer's barrier integrity and respiratory activity. Predicted influences of the electron transport chain modulators, antimycin A and malonoben, as well as the cytoskeleton active cytochalasin D, were clearly reproduced by TER-Ox readings. Thus, the use of TER-Ox assays offers the possibility to determine influences on barrier function and respiratory activity of the identical cell population, leading to more reliable, fact-based, multi-parametric interpretation of the observed biological response. Additionally, the simultaneous quantification of both parameters, TER and AOCR, results in a reduction of assay time and cost. The imaging approach used for monitoring oxygen consumption might also be used to determine local changes in respiratory activity within a mixed 2D cell layer, for example in coculture models. Finally, the setup is adaptable to higher throughputs, which is particularly important to become attractive for screening campaigns.

Acknowledgements

The authors would like to thank the machine workshop of the chemistry department of the University of Regensburg for their great support during the development of the experimental TER-Ox setup. The authors would like to acknowledge funding by the *Deutsche Forschungsgemeinschaft* DFG within the collaborative research center *TRR 305* (project number 429280966). Open Access funding enabled and organized by Projekt DEAL.

Conflicts of Interest

The authors declare no conflicts of interest.

Data Availability Statement

Data is available from the corresponding author upon reasonable request.

References

1. R. Kalluri and R. A. Weinberg, "The Basics of Epithelial-Mesenchymal Transition," *Journal of Clinical Investigation* 119 (2009): 1420–1428.

2. S. Lovisa, "Epithelial-to-Mesenchymal Transition in Fibrosis: Concepts and Targeting Strategies," *Frontiers in Pharmacology* 12 (2021): 737570.

3. S. Lamouille, J. Xu, and R. Derynck, "Molecular Mechanisms of Epithelial–Mesenchymal Transition," *Nature Reviews Molecular Cell Biology* 15 (2014): 178–196.

4. M. Sciacovelli and C. Frezza, "Metabolic Reprogramming and Epithelial-to-Mesenchymal Transition in Cancer," *FEBS Journal* 284 (2017): 3132–3144.

5. J. Caines, D. Barnes, and M. Berry, 2022. Methods in Molecular Biology 2508225–234.

6. A. S. Divakaruni and M. Jastroch, "A Practical Guide for the Analysis, Standardization and Interpretation of Oxygen Consumption Measurements," *Nature Metabolism* 4 (2022): 978–994.

7. M. Brischwein, J. Wiest, and J. Wegener, Ed. in Bioanalytical Reviews in Label-Free Monitoring of Cells in vitro 2 (2019) 163–188.

8. S. Sheridan, S. Gil, M. Wilgo, and A. Pitt, 2008. Methods in Cell Biology 8629–57.

9. A. Hakvoort, M. Haselbach, J. Wegener, D. Hoheisel, and H. J. Galla, "The Polarity of Choroid Plexus Epithelial Cells In Vitro Is Improved in Serum-Free Medium," *Journal of Neurochemistry* 71 (1998): 1141–1150.

10. B. Press and D. Di Grandi, "Permeability for Intestinal Absorption: Caco-2 Assay and Related Issues," *Current Drug Metabolism* 9 (2008): 893–900.

11. A. Avdeef, M. Deli, and W. Neuhaus, *L. Di and E. H. Kerns*, Eds. in in Blood-Brain Barrier in Drug Discovery (2015) 188–237.

12. J. D. Irvine, L. Takahashi, K. Lockhart, et al., "MDCK (Madin-Darby Canine Kidney) Cells: A Tool for Membrane Permeability Screening," *Journal of Pharmaceutical Sciences* 88 (1999): 28–33.

13. B. Srinivasan, A. R. Kolli, M. B. Esch, H. E. Abaci, M. L. Shuler, and J. J. Hickman, "TEER Measurement Techniques for In Vitro Barrier Model Systems," *SLAS Technology* 20 (2015): 107–126.

14. B. Jovov, N. K. Wills, and S. A. Lewis, "A Spectroscopic Method for Assessing Confluence of Epithelial Cell Cultures," *American Journal of Physiology-Cell Physiology* 261 (1991): C1196–C1203.

15. N. J. Douville, Y.-C. Tung, R. Li, J. D. Wang, M. E. H. El-Sayed, and S. Takayama, "Fabrication of Two-Layered Channel System With Embedded Electrodes to Measure Resistance Across Epithelial and Endothelial Barriers," *Analytical Chemistry* 82 (2010): 2505–2511.

16. J. Wegener, D. Abrams, W. Willenbrink, H.-J. Galla, and A. Janshoff, "Automated Multi-Well Device to Measure Transepithelial Electrical Resistances Under Physiological Conditions," *Biotechniques* 37 (2004): 590–597, 592-4, 596-7.

17. D. Marrero, F. Pujol-Vila, D. Vera, et al., "Gut-on-a-Chip: Mimicking and Monitoring the Human Intestine," *Biosensors and Bioelectronics* 181 (2021): 113156.

18. S. Fuchs, S. Johansson, A. Ø. Tjell, G. Werr, T. Mayr, and M. Tenje, "In-Line Analysis of Organ-on-Chip Systems With Sensors: Integration, Fabrication, Challenges, and Potential," *ACS Biomaterials Science & Engineering* 7 (2021): 2926–2948.

19. F. Urban, K. Hajek, T. Naber, B. Anczykowski, M. Schäfer, and J. Wegener, "Peter-Assay: Combined Impedimetric Detection of Permeability (PE) and Resistance (TER) of Barrier-Forming Cell Layers," *Scientific Reports* 10 (2020): 7373.

20. M. I. Hermanns, R. E. Unger, K. Kehe, K. Peters, and C. J. Kirkpatrick, "Lung Epithelial Cell Lines in Coculture With Human Pulmonary Microvascular Endothelial Cells: Development of an Alveolo-Capillary Barrier in Vitro," *Laboratory Investigation* 84 (2004): 736–752.

21. H. Ren, N. P. Birch, and V. Suresh, "An Optimised Human Cell Culture Model for Alveolar Epithelial Transport," *PLoS One* 11 (2016): e0165225.

22. J. Wegener, S. Zink, P. Rösen, and H. J. Galla, "Use of Electrochemical Impedance Measurements to Monitor β-adrenergic Stimulation of Bovine Aortic Endothelial Cells," *Pflugers Archiv European Journal of Physiology* 437 (1999): 925–934.

23. L. J. Gentet, G. J. Stuart, and J. D. Clements, "Direct Measurement of Specific Membrane Capacitance in Neurons," *Biophysical Journal* 79 (2000): 314–320.

24. J. D. Dukes, P. Whitley, and A. D. Chalmers, "The MDCK Variety Pack: Choosing the Right Strain," *BMC Cell Biology* 12 (2011): 43.

25. K. Hajek and J. Wegener, "Independent Impedimetric Analysis of Two Cell Populations Co-Cultured on Opposite Sides of a Porous Support," *Experimental Cell Research* 351 (2017): 121–126.

26. B. R. Stevenson, J. M. Anderson, D. A. Goodenough, and M. S. Mooseker, "Tight Junction Structure and ZO-1 Content Are Identical in Two Strains of Madin-Darby Canine Kidney Cells Which Differ in Transepithelial Resistance," *Journal of Cell Biology* 107 (1988): 2401–2408.

27. B. A. Wagner, S. Venkataraman, and G. R. Buettner, "The Rate of Oxygen Utilization by Cells," *Free Radical Biology and Medicine* 51 (2011): 700–712.

28. T. W. Molter, M. R. Holl, J. M. Dragavon, et al., "A New Approach for Measuring Single-Cell Oxygen Consumption Rates," *IEEE Transactions on Automation Science and Engineering* 5 (2008): 32–42.

29. D. Hoheisel, T. Nitz, H. Franke, et al., "Hydrocortisone Reinforces the Blood–Brain Barrier Properties in a Serum Free Cell Culture System," *Biochemical and Biophysical Research Communications* 244 (1998): 312–316.

30. E. C. Slater, "The Mechanism of Action of the Respiratory Inhibitor, Antimycin," *Biochimica et Biophysica Acta (BBA) - Reviews on Bioenergetics* 301 (1973): 129–154.

31. H. Terada, "Uncouplers of Oxidative Phosphorylation," *Environmental Health Perspectives* 87 (1990): 213–218.

32. M. Schliwa, "Action of Cytochalasin D on Cytoskeletal Networks," *Journal of Cell Biology* 92 (1982): 79–91.

Supporting Information

Additional supporting information can be found online in the Supporting Information section.